ADVANCED MATERIALS
www.advmat.de

Synergistic Gating of Electro-Iono-Photoactive 2D Chalcogenide Neuristors: Coexistence of Hebbian and Homeostatic Synaptic Metaplasticity

*Rohit Abraham John, Fucai Liu, Nguyen Anh Chien, Mohit R. Kulkarni, Chao Zhu, Qundong Fu, Arindam Basu, Zheng Liu, and Nripan Mathews**

Emulation of brain-like signal processing with thin-film devices can lay the foundation for building artificially intelligent learning circuitry in future. Encompassing higher functionalities into single artificial neural elements will allow the development of robust neuromorphic circuitry emulating biological adaptation mechanisms with drastically lesser neural elements, mitigating strict process challenges and high circuit density requirements necessary to match the computational complexity of the human brain. Here, 2D transition metal di-chalcogenide (MoS_2) neuristors are designed to mimic intracellular ion endocytosis–exocytosis dynamics/neurotransmitter-release in chemical synapses using three approaches: (i) electronic-mode: a defect modulation approach where the traps at the semiconductor–dielectric interface are perturbed; (ii) ionotronic-mode: where electronic responses are modulated via ionic gating; and (iii) photoactive-mode: harnessing persistent photoconductivity or trap-assisted slow recombination mechanisms. Exploiting a novel multigated architecture incorporating electrical and optical biases, this incarnation not only addresses different charge-trapping probabilities to finely modulate the synaptic weights, but also amalgamates neuromodulation schemes to achieve "plasticity of plasticity–metaplasticity" via dynamic control of Hebbian spike-time dependent plasticity and homeostatic regulation. Coexistence of such multiple forms of synaptic plasticity increases the efficacy of memory storage and processing capacity of artificial neuristors, enabling design of highly efficient novel neural architectures.

In contrast to the conventional serial processing achieved with today's von Neumann architectures, the human brain utilizes highly parallel, event-driven, and energy-efficient architectures to achieve computational power of the order of 10^{18} FLOPS at a power consumption of ≈20 W.[1] With ≈86 billion neurons in synaptic communication making 10 quadrillion calculations every second, our brain possesses an unmatched parallel processing power with 17.2 trillion action potentials per second.[2] Learning in the brain happens through modification of synaptic weights through processes such as long-term potentiation and depression.[3] Typical cortical neurons have one to ten thousand synaptic connections which operate by electrochemical signaling using neurotransmitters. For optimum firing, the neuronal dynamics maintains a balanced excitatory status quo via an integration/summation process combined with a mechanism that triggers action potentials above a threshold voltage, as per the leaky Integrate-And-Fire Model.[4] To mimic these neuronal dynamics; conductance change (synaptic weight) of the artificial synaptic circuits has to be tuned continuously to demonstrate plasticity and nonvolatility.[5] Mimicking synaptic signal transmission through nanoelectronic circuits thus becomes the cardinal research target in the field of neuromorphic engineering. However, hardware implementation of neural networks emulating synaptic functionalities with comparable complexity and feasible power dissipation remain exceptionally challenging. Neuromorphic circuitry based on conventional silicon-complementary metal–oxide–semiconductor (CMOS) technology using memory to store synaptic weights require additional clock cycles to update the weights, thereby imposing issues with power consumption and scalability.[6] Memristors[7,8] with programmable resistance states which are presently in focus, are compromised by excessive write-noise nonlinearities and abrupt conductance transitions which limit the programmable states (and hence accessible synaptic weights). From a technological perspective, highly stringent process requirements and device integrity expectations further worsens the

R. A. John, Dr. F. Liu, Dr. N. A. Chien, M. R. Kulkarni, C. Zhu, Q. Fu, Prof. Z. Liu, Prof. N. Mathews
School of Materials Science and Engineering
Nanyang Technological University
50 Nanyang Avenue, Singapore 639798
E-mail: Nripan@ntu.edu.sg
Prof. A. Basu
School of Electrical and Electronic Engineering
Nanyang Technological University
50 Nanyang Avenue, Singapore 639798
Prof. N. Mathews
Energy Research Institute @ NTU (ERI@N)
Nanyang Technological University
Singapore 637553
The ORCID identification number(s) for the author(s) of this article can be found under https://doi.org/10.1002/adma.201800220.

DOI: 10.1002/adma.201800220

challenge of fabricating high-density circuitry necessary to match the degree of complexity and number of neurons in the human brain.[9–11] An alternative strategy to this would be to incorporate augmentative functionalities into a single neural element to enhance the achievable plasticity and parallelism. This would allow the development of robust neuromorphic circuitry emulating biological adaptation mechanisms with drastically lesser neural elements, mitigating strict process and density requirements. With an additional gate-control, thin-film transistors (TFTs) based on organic[12,13] and inorganic semiconductors[14–16] seems promising in this regard, exploiting hysteresis to achieve dynamic, linear plasticity when compared to abrupt state transitions in a memristor. The degree of such trapping and electrostatic doping–dedoping can be maximized with ultra-thin semiconducting channels encompassing intimate ionic/electronic coupling at the semiconductor–dielectric interface. Additionally, optical control of synaptic weights can help unlock novel neural network architectures with global connectivity, overcoming interconnect limitations, mitigating thermal loss and improving the signal-to-noise ratio. This calls for the need of atomically thin semiconducting channels with optoelectronically modulatable carrier concentration, and synergistic gating strategies to probe various trapping probabilities and hence the memresistance states in these semiconductors.

Two-dimensional (2D) transition metal di-chalcogenides (TMDCs) with their ultrafast charge carrier dynamics[17,18] and atomic scalability[19] present a platform with highly modulatable optoelectronic transitions[20,21] that could overcome the limitations of previously investigated material classes. Here, we investigate optoelectronic synaptic plasticity in molybdenum disulfide (MoS_2) three-terminal devices via three gating approaches and synergistic combinations thereof. Different trapping probabilities are addressed via individual/combined gating techniques, tuning synaptic weights with higher modulability and homeostatic stability. Initial training sequences created short-term changes in the device conductance/weights, which consolidated to long-term plasticity with persistent instructions. Controlled facilitation/depression was achieved through the multigated architecture, with the three modes operating additive/subtractive to each other. Additive operation strengthened the degree of weight plasticity, while subtractive operation regulated these weight changes through a negative feedback mechanism called homeostatic plasticity. Coexistence of Hebbian and homeostatic plasticity not only helped prevent runaway excitation during elevated excitability, but also increased synaptic gain and impeded unnecessary synapse silencing during chronic activity suppression,[22] enabling design of highly efficient novel neural architectures. Finally, a classical-conditioning experiment (Pavlov's dog) is realized utilizing concurrent optoelectronic activation, demonstrating a basic form of associative-memory in our systems. These comprehensive results benchmark the possible gating approaches required to achieve parallelism and open up new possibilities of multigated neural architectures with 2D chalcogenides as a viable material platform.

Figure 1A–C illustrates the steps in biological synaptic transmission, the proposed multigate device architecture, and an analog circuitry depicting interplay between Hebbian and Homeostatic synaptic plasticity, respectively. Devices operating in electronic-mode utilized a bottom-gate top-contact configuration with silicon dioxide (SiO_2) as the dielectric, while ionotronic-mode was enabled by an ionic liquid [*N*,*N*-diethyl-*N*-(2-methoxyethyl)-*N*-methyl-ammonium-bis-(trifluoromethylsulfonyl)-imide (DEMETFSI)] contact. Device fabrication and physical characterizations are described in detail in the Experimental Section and Note S1 and Figure S1 of the Supporting Information. Both modes exhibited typical n-type depletion-operation with electronic-mode depicting a linear mobility of 28 $cm^2\ V^{-1}\ s^{-1}$ when compared to 14.6 $cm^2\ V^{-1}\ s^{-1}$ for ionotronic-mode. Interestingly, while devices in the electronic-mode depicted a distinct clockwise hysteresis window of 8 V indicating trapping and detrapping of electrons in the forward and reverse voltage scans;[24] ionotronic-mode operation exhibited an anticlockwise hysteresis window of 0.5 V signifying ion-related electric-double-layer modulation in the system[25] (Note S2 and Figure S2, Supporting Information). Different trapping possibilities were utilized in both configurations to mimic the ion flux and neurotransmitter release dynamics in chemical synapses. The synaptic transmission steps illustrated in Figure 1A is explained in detail in Note S3 of the Supporting Information. For the synaptic three-terminal devices, gate terminal served as the presynaptic input while the semiconducting 2D TMDC channel with source/drain electrodes were furnished as postsynaptic output terminals. Interfacial traps (electronic-mode)/ions in the ionic liquid (ionotronic-mode) mimicked neurotransmitters, while channel conductance served as the synaptic weight.

To demonstrate comprehensive emulation of synaptic signatures and mimic the essential features of neurotransmitter release, namely, excitatory or inhibitory,[26] quantal,[27] and probabilistic,[28] postsynaptic responses (I_{ds}) triggered by presynaptic pulses (V_g) were recorded as a function of pre- and postsynaptic pulse width, pulse interval, frequency, and number of repetitions. A combination of these three emulated the cellular machinery responsible for short- and long-term synaptic plasticity. Chemical synapses via expression of facilitation and depression mechanisms, create short and long-term plastic changes within neurons according to the dual-process theory of plasticity.[29] As explained in Note S3 of the Supporting Information, arrival of an action potential depolarizes the synaptic membrane, causing influx of Ca^{2+} into the presynaptic membrane. When triggered immediately by a temporally correlated action potential, residual Ca^{2+} concentration from the first pulse augments the Ca^{2+} activated by the second pulse, thereby increasing the vesicular release probability and resulting in facilitation. This phenomenon called neural facilitation/paired-pulse facilitation (PPF)[30] was emulated by evoking excitatory postsynaptic currents (EPSCs)[31] in response to paired presynaptic spikes as shown in Note S4, Figure S3, and Table S1 of the Supporting Information. Small pulse intervals (<30 ms) triggered EPSCs with higher strength when compared to the priori spikes resulting in a strong facilitation index ≫100%. Slower ion relaxation kinetics in the ionotronic-mode enhanced this facilitation index depicting a higher ratio of ≈206% when compared to 165% for the electronic-mode. Larger pulse intervals weakened this augmentation with the PPF index reaching around 100% for a pulse interval of 500 ms. Such temporal enhancement of synaptic connections mimicked the excitatory nature of neurotransmitter release,[26,32] analogous to glutamatergic systems, resulting in short-term potentiation (STP).[33] Similar activation by inhibitory presynaptic spikes resulted

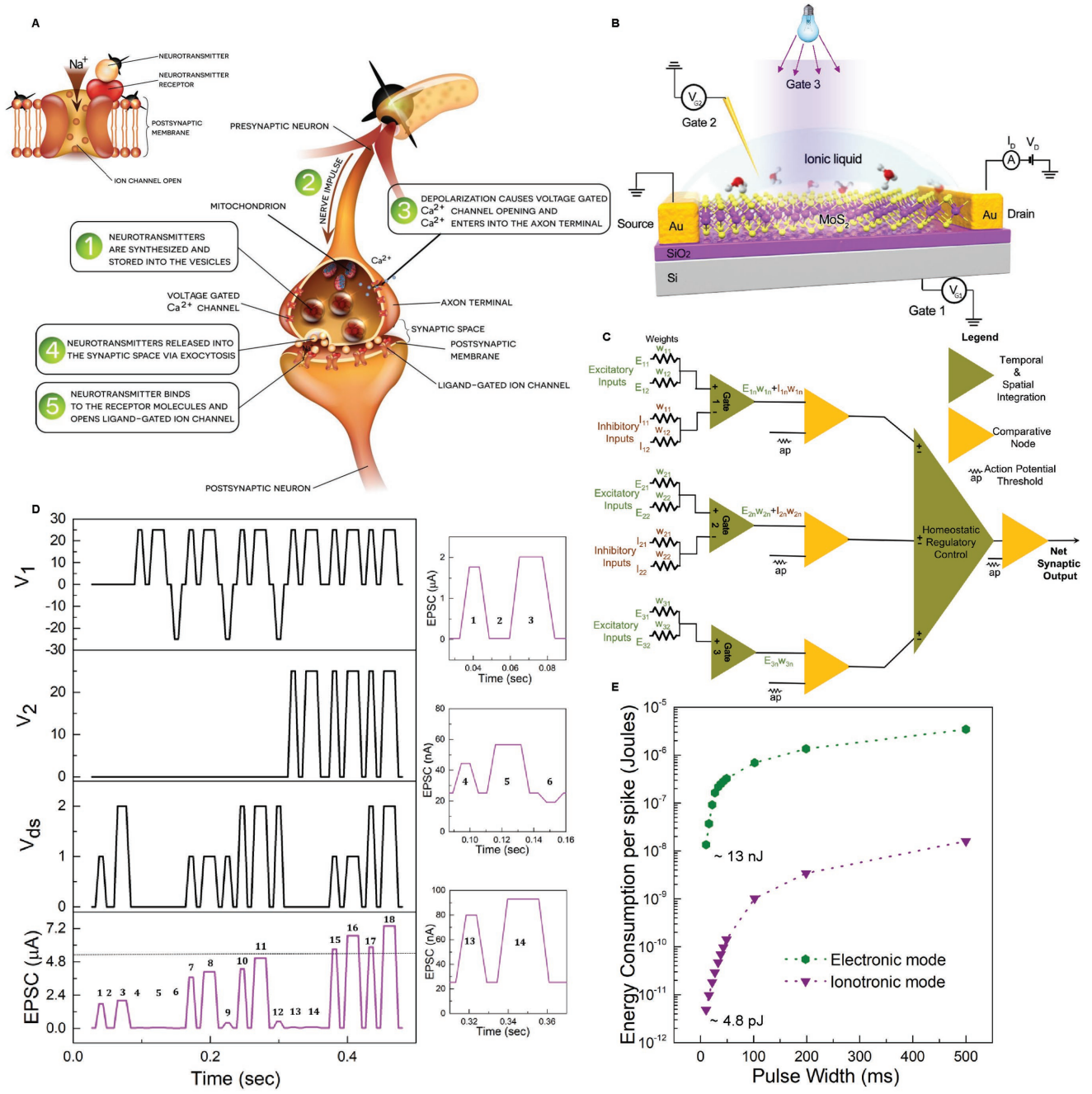

Figure 1. Mimicking synaptic transmission using MoS_2 neuristors. A) Schematic of biological synaptic transmission. B) The proposed multigated architecture of analogous artificial MoS_2 synapses. C) Analog circuit depicting interplay between Hebbian and Homeostatic synaptic plasticity. D) Dendritic integration-based spiking logic response driven by two presynaptic driving inputs V_1 and V_2, and a modulatory input V_{ds}. Images on the right side represent magnified views of high impedance resistance states. The dotted line represents the threshold current level (5.5 μA) defining logic states "1" and "0." E) Comparison of the ON-state energy consumption per spike (E_{on}) of the MoS_2 synapses as a function of presynaptic pulse width in the electronic and ionotronic-modes. E_{on} was calculated from the equation[23] $E_{on} = I_{peak} \times t \times V$, where I_{peak} is the maximum value of generated EPSC, t is the spike duration, and V is the applied drain voltage. Further scaling down of device dimensions and reducing spike durations to sub-millisecond levels could be utilized as strategies to bring down the energy consumption per event.

in short-term depression (STD) (Note S4 and Figure S3, Supporting Information). In the electronic-mode, the spiking rise and decay in EPSCs was caused by electron trapping–detrapping at the semiconducting channel, while ion migration–relaxation kinetics at the ionic liquid–semiconductor interface (Helmholtz double layer) accounted for this phenomenon in the ionotronic-mode. For PPF in the electronic/ionotronic-mode, when the pulse interval was shorter than relaxation time of trapped electrons/mobile cations, some of these trapped electrons/ions were unable to return to their equilibrium positions

before the second spike was initiated. As a result, these residual electrons/cations induced additional charges in the channel, leading to an increase in channel current and higher PPF index. Large pulse interval allowed these mobile electrons/cations to relax back to their equilibrium positions prior to the second spike application leading to weak channel current modulation and lower PPF index.[16]

Extending the STP behavior, quantal release[27] of neurotransmitters in a chemical synapse was captured as postsynaptic weight changes in response to frequency dependent action potentials. Dynamic frequency dependent filters[34] established causal relations between neighboring neurons, with specific temporal patterns of activity in neural network. Both electronic and ionotronic-modes exhibited high frequency facilitation characteristics analogous to synapses with low initial probability of vesicle release. Similarly, short-term synaptic depression could be represented by low-pass temporal filters.[35] These were in turn integrated with an external microcontroller circuitry and a photoresistor for obstacle detection as explained in (Note S4 and Figure S4, Supporting Information). An obstacle proximity of <2 cm caused conductance changes to the photoresistor, in turn triggering presynaptic firing rate at 45 Hz via a processing circuit, resulting in temporal neural spiking activity with a gain of 1.86 and 16.51 for the electronic and ionotronic-modes, respectively (Figure S4B,C, Supporting Information). The quantal neurotransmitter release model assumes finite number of neurotransmitters per synaptic vesicle, where the final EPSC is the sum of activated miniature EPSCs. Increment in EPSCs as a function of presynaptic pulses number modeled the increase in neurotransmitter release and strengthening of synaptic connections with higher number of action potentials. The obtained learning curves followed an exponential growth behavior as postulated by Ebbinghaus (Note S4 and Figure S5, Supporting Information) and depicted a progressive enforcement of synaptic activity, related to learning process and memory recall.[36]

In a neuron, spatiotemporal summation of action potentials triggers a singular change in membrane potential, as per the "integrate and fire neuron model."[37,38] Here, we utilize multiple presynaptic gate inputs (two driving inputs V_1 and V_2 and one modulatory input (V_d/V_{ds}), to demonstrate a neuronal arithmetic with dynamic spiking logic "OR" and "AND" operations in the electronic-mode, akin to dendritic integration in neurons (Figure 1D). Logic states 1 to 3 represented strong modulation of postsynaptic responses as a function of the modulatory input V_{ds}. This also accounted for the multiplicative neural logic depicted in Figure S6A of the Supporting Information. Asynchronous firing or absence of any of the three inputs resulted in logic "OR" operation (Logic states 1–15), with PSCs failing to cross the threshold of activation (5.5 μA). However, with synchronous firing of the driving inputs V_1, V_2, and the modulatory input V_{ds}, the cumulative PSC increased to a level above the threshold, thereby demonstrating logic "AND" operation (Logic states 15–18), mimicking ion migration across the synaptic membrane causing membrane depolarization. PSC modulation with duty cycle of the inputs, presented in logic states (4–5, 7–8, and 10–11) could be used to design frequency modulated coding schemes, while PSC modulation with presynaptic pulse amplitudes and polarity could be useful for amplitude modulated information coding schemes. With additional drain terminal control, neuronal logic with dynamic gain modulation was realized here with the vesicular release probability being defined by V_{ds} and pulse width of the firing inputs. In accordance with the probabilistic release model,[28] modulation of EPSCs as a function of pulse width of the presynaptic spikes (defined as Spike-duration-dependent plasticity[39]) established temporal causality and feedback for dynamically regulating the vesicular release probability. Increase in V_{ds} dynamically tuned the measured sum exhibiting superlinear behavior as depicted in Note S5 and Figure S6 of the Supporting Information. Positive V_{ds} enhanced the neuronal gain while left-shift of the x-axis intercept changes represented additive operation.[40,41]

Despite remarkable progress in emulating synaptic characteristics, current artificial synapses still consume energy that is orders of magnitude greater than their biological counterparts (≈10 fJ per synaptic event[42]). Hence, reduction of energy consumption is a primary concern. On comparing the configurations, ionotronic-mode operated at significantly lower power (≈4.8 pJ per event) than the electronic-mode (≈13 nJ per event), when triggered with the same presynaptic spike (pulse width = 10.5 ms) (Figure 1E; Note S6 and Table S2, Supporting Information). Although still considerably higher than the energy consumption of chemical synapses, ion-mediated gating/ionotronic-mode seems promising in this regard and provides a significant step toward realizing ultralow power artificially intelligent electronics. Other recently developed architectures involving stacked hexagonal boron nitride–molybdenum disulfide (MoS_2) could allow access to even lower power operation in future.[43] Using a future scaled version of these MoS_2 neuristors (active area = 1 μm^2), the energy consumption per write will account to only 26.67 fJ, better than state-of-the-art memristors[44] and simulated spintronic domain-wall magnets for spiking neural networks.[45]

Leveraging on the comprehensive emulation of short-term synaptic signatures, various gating strategies were designed to program the synaptic weights to achieve nonvolatility and long-term plasticity, essential for neuromorphic computing algorithms. While the hybrid ionic-electronic approaches utilized trapping probabilities at the semiconductor–dielectric interface to achieve hysteresis; a novel optical gating approach (photoactive-mode) utilizing defect-assisted slow recombination mechanisms was harnessed next to create long-term changes in the synaptic weight. These approaches were then conclusively combined to tune the synaptic weight with higher modulability and homeostatic stability.

Electrical programming of synaptic weights: Persistent activity-dependent changes in synaptic transmission, such as long-term potentiation (LTP) and long-term depression (LTD), are thought to play a critical role in learning and subsequent memory formation. Understanding LTP and LTD reflects how long-lasting memory-associated changes are likely to occur in the central nervous system and yield valid insights into the underlying cellular mechanism of learning and memory. In glutamatergic systems, LTP is caused due to high frequency activation of Mg^{2+} sensitive N-methyl-D-aspartate receptors and phosphorylation of α-amino-3-hydroxy-5-methyl-4-isoxazolepropionic acid (AMPA) receptors, resulting in large

ion influx (Na^+, K^+, and Ca^{2+}) into the synaptic membranes, creating a larger postsynaptic dendritic spine with an enhanced synaptic strength.[46] In opposition to potentiation, depression decreases the efficacy of a synapse via low frequency activation of phosphatases causing internalization of AMPA receptors through dephosphorylation. In this study, LTP and LTD were induced via repeated presynaptic training pulses at the gate terminal. Long-term measurements were conducted on fresh samples to avoid effects of history affecting the experiment. While persistent pulsing at −50 V activated LTP in the electronic-mode, +2 V activated LTP in the ionotronic-mode. A linear increase in weights was observed with increased number of training pulses. Application of 100 facilitating pulses resulted in a weight change of 117% in the electronic-mode, while a larger increment of 223% was observed in the ionotronic-mode (**Figure 2**A,B,E). Application of reverse potential resulted in depression or decrease in conductance, the degree of which was again dependent on the total duration of pulsing/biasing and amplitude of the reverse potential. Electronic-mode depicted a higher depression rate with a weight change of 69% when compared to 54% in the ionotronic-mode. Similar to short-term plasticity, persistent voltage pulses trapped large number of charge carriers at the semiconductor–dielectric interface resulting in the positive (LTP)/negative (LTD) shift of the conductivity depending on the configuration.[24,25,47] Application of opposite-polarity pulses resulted in removal of the trapped electrons leading to a reversal in the observed phenomena. Scanning rates were kept constant in all these measurements to avoid interference of any scanning-rate dependent hysteresis. Such time-dependent channel hysteretic behavior due to charge-trapping dynamics has been previously observed in 2D TMDC-based TFTs via current transient measurements.[47,48] Normalizing to the same writing time, the ionotronic-mode depicted larger retention characteristics indicating slower carrier relaxation dynamics in this mode of operation.

Optical programming of synaptic weights: The highly modulatable photogenerated carrier concentration in atomically thin 2D chalcogenide channels[49,50] (here MoS_2) unlocks the possibility of addressing synaptic weights with photon pulses, capitalizing on high-bandwidth optical communication protocols. Here, a very strong LTP was induced in our devices via a novel optical gating approach (photoactive-mode), with light pulses (λ = 445 nm) serving as the presynaptic inputs. Upon illumination, the conductance increased rapidly initially and then gradually reached ≈1 order of magnitude above the dark current. On termination of optical illumination, the conductance exhibited a rapid drop, but remained in a high conductance state as depicted in Figure 2C, and Note S7 and Figure S7B,C of the Supporting Information. The rapid transitions were attributed to band-to-band transitions, while the long-lasting high conductance change called persistent photoconductivity (PPC)[51] was attributed to defect or trap centered slow recombination in accordance with the random local potential fluctuation (RLPF) model.[52] Slower decay marked by increased decay times with increasing photon dosage also agreed well with the RLPF model, with more carriers occupying the sites of the local potential minima resulting in a slower recombination. Here, PPC was harnessed to create permanent changes in postsynaptic conductance as shown in Figure 2C. Increased photodose enhanced device conductance and modulated the decay dynamics. For the highest photodose, the device remained in a high-conductivity state (>/= 2.7 μA) for a period >2 h, thereby emulating time-dependent stabilization from STP to LTP, called "consolidation"[53] in human brain, in congruence with "the multistore model" of human memory by Atkinson and Shiffrin.[8] Utilization of such photon pulses would help unlock novel neural network architectures where light could be used as a global gate to selectively activate a patch of light sensitive neurons interspersed between photo-insensitive neural elements. This design would also enable architectures with far less number of interconnects, mitigating thermal loss and stray signals, hence improving the signal-to-noise ratio. However, eliminating light induced parasitic currents in hybrid-CMOS neural network architectures would remain challenging and would require additional reflective metal shielding structures to block the light from underlying silicon substrate.

Synergistic gating enables "plasticity of plasticity–metaplasticity" via interplay between Hebbian plasticity and Homeostatic feedback regulation.[54] Temporal correlations between the pre- and postsynaptic spikes created voltage and time dependent weight changes in conductivity, establishing various forms of spike-timing-dependent plasticity (STDP) rules in our systems. A refinement of Hebb's theory, STDP is considered to be the first law of synaptic plasticity and is believed to underlie learning and memory by competitive strengthening and weakening of synapses in neural networks.[55] In glutamatergic connections, strengthening/LTP occurs if the presynaptic action potential precedes the postsynaptic firing ($t_{post-pre} > 0$, where δt is the relative time interval between the pre- and the postsynaptic spikes), while presynaptic potentials following postsynaptic spikes ($t_{post-pre} < 0$) causes weakening/LTD. While operation in the electronic-mode helped realize asymmetric Hebbian STDP protocol, ionotronic-mode operation resulted in "reverse" STDP/asymmetric anti-Hebbian STDP protocol, reflecting coexistence of different coupling mechanisms within the same device (Figure 2D; Note S8 and Figure S8, Supporting Information).[56] Coexistence of such multiple forms of synaptic plasticity increases the efficacy of memory storage and processing capacity of artificial neuristors, enabling design of highly efficient novel neural architectures. These distinct types of parallel synaptic plasticity also reflect specific subcellular molecular prerequisites and depend on background brain activity states. For example, dopamine and brain-derived neurotrophic factor modulates unique hippocampal STDP at Schaffer collateral-CA1 synapses.[57] To the best of our knowledge, this is the first demonstration of interplay between multimodal synaptic signatures achieved in a single neural element. Moreover, different trapping probabilities could be coupled to further fine-tune weight changes achieved during facilitation and depression, emulating different molecular pathways and neuromodulators for induction and expression of STDP. This plasticity of plasticity or metaplasticity demonstrated here reflects a dynamic regulation of plasticity via an internal modulation mechanism maintaining the synaptic efficacy within a dynamic range.[54] For example, additive operation of electronic and ionotronic-modes in a dual-gated approach enhanced the degree of facilitation/depression as shown in Figure 2E. The weight changes increased with a higher slope of 3.13 when compared to 1.24 and 1.88 for

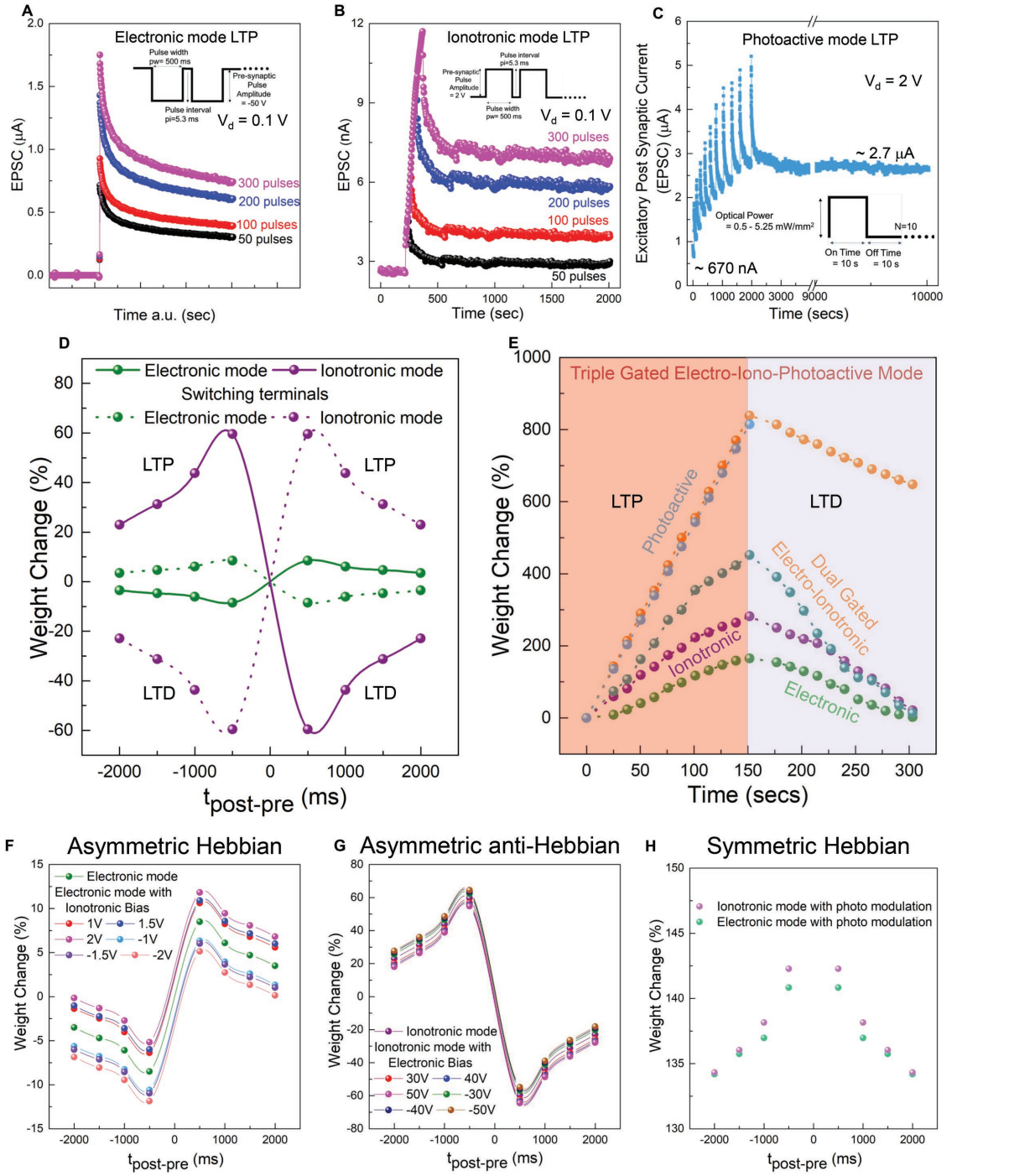

Figure 2. Interplay between Hebbian and Homeostatic synaptic plasticity in MoS_2 neuristors. Increment in long-term potentiation (LTP) strength as a function of persistent training in (A) electronic-mode (magnified view). Refer to Figure S7A of the Supporting Information for nonmagnified view. B) Ionotronic-mode (C) photoactive-mode (variation with increment in light intensity 0.5–5.25 mW mm^{-2}). D) Spike-timing-dependent plasticity (STDP) and "reverse" STDP (rSTDP) achieved with the electronic and ionotronic-modes, respectively. Differences in trapping probabilities modulated the PSCs and relative timing between the output and the input spikes modified the strength of synaptic weights through facilitation and depression. Reversal of pre- and postsynaptic terminals resulted in reversal of the STDP protocols, as indicated by the dotted lines. E) Controlled facilitation and depression achieved in our devices with the multigated architecture. STDP modulation and homeostatic regulation in (F) electronic (Asymmetric Hebbian) and (G) ionotronic-mode (Asymmetric anti-Hebbian) of operation. H) Symmetric Hebbian STDP protocol observed in the photoactive-mode of operation.

purely electronic and ionotronic-modes, respectively. Subtractive mode of operation helped stabilize weight changes in the STDP protocols, analogous to homeostatic negative feedback regulation[58] in biological neural network. Recent findings have revealed homeostatic mechanism to be an on-demand rapid tuning of synaptic strengths in contrast to the popular view of

a slow, global phenomenon.[59] Analogous to this, subtractive operation of the several modes was utilized to create a negative feedback mechanism to offset excessive excitation or inhibition by adjusting their synaptic strengths. For example, the device could be configured in a double-gated mode where facilitation caused by electronic-mode could be counteracted by depression of ionotronic-mode and vice versa (Figure 2F,G). Thus, based on the net coupling of carriers, corresponding weight changes could be programmed with fine precision. Similarly, operation in photoactive-mode depicted very strong facilitation signatures analogous to runaway dynamics[60] of synaptic weights, but could be regulated by negating homeostatic regulatory electronic and ionotronic-mode of operation via a negative feedback mechanism (Figure 2E). Large facilitation in photoconductance (>800%) was regulated by 22% depression activated by combinatorial operation of electronic and ionotronic-modes within a timescale of 150 s. Staying within this time frame, the corresponding STDP protocol exhibited a net facilitation independent of relative time interval between the pre- and the postsynaptic voltage spikes, viz., a symmetric Hebbian STDP behavior (Figure 2E,H). Complete homeostatic compensation was possible at larger timescales (≈900 s). Thus, the positive feedback process of Hebbian plasticity with associative synaptic changes could be regulated by a homeostatic negative feedback process, constraining activity levels and maintaining stability all within a single neural element. With combination of a low intensity photodose and high counteracting electrical erasing voltages, it becomes possible to tune this behavior even further. To the best of our knowledge, this is the first demonstration of interplay between Hebbian and Homeostatic plasticity in a single artificial neural element. Compared to previous works on metaplasticity in memristors that used only presynaptic activity-based priming,[61,62] a new terminal that may be controlled by presynaptic rate or other signals such as similar to neuromodulation by dopaminergic, noradrenergic, muscarinic, and nicotinic receptors[63,64] is realized here. This control gate may also be used to induce homeostasis, enabling neural network operation within its normal dynamic range.[65,66] Hence, this multigated optoelectronic approach enables novel artificial neural architectures with multiple operational modes and theoretically infinite plasticity. However, it should be noted that in practical implementations of the multigated approach with metaplasticity, the synapse needs to be disconnected from the neuron on a postsynaptic spike, as is commonly done in other nonvolatile memory-based synaptic plasticity[5,56,67,68] to prevent large surges in EPSCs due to any individual gating inputs from affecting the network dynamics.

Finally, the famous classical conditioning Pavlov's dog experiments[69,70] (**Figure 3**; Note S9 and Figure S9, Supporting Information) were conducted to emulate associative learning in the human brain. In comparison to Pavolovian memristors[69] with temporal dependence of activation signals, this study implements classical conditioning in a thin-film transistor configuration with intimate coupling between optical and

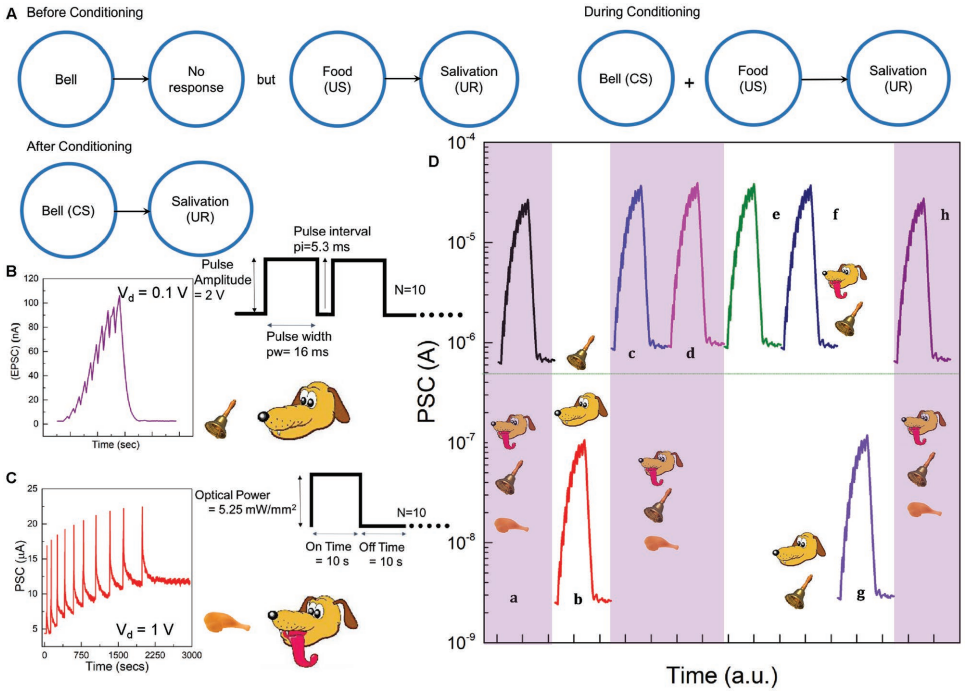

Figure 3. Classical conditioning Pavlov's dog experiment. A) Schematic representing outline of Pavlov's dog experiment. B) Voltage pulses/conditioned stimulus (CS), (C) optical pulses/unconditioned stimulus (US), and their responses. D) Classical conditioning demonstrated by Pavlov's dog experiment. Initially, light pulses (unconditioned stimulus) led to an efficient unconditioned response (salivation) (state a). However, voltage pulses to the back gate (conditioned stimulus) did not lead to an efficient conditioned response before training (current < 500 nA, no salivation). Initial training sequences with conditioned and unconditioned stimuli did not result in effective association as depicted by state b. Repeated training led to strong association, after which conditioned stimulus alone could trigger salivation (states c–f, current > 500 nA). However, the PSCs decreased below the salivation threshold when triggered by conditioned stimulus alone without accompanying unconditioned stimulus for ≈2 h, indicating extinction of associative memory (state g). Finally, the association was recovered back faster with simultaneous conditioned and unconditioned stimuli (state h).

electrical pulses, unlocking novel neural network architectures with light as a global gate. Here, light pulses emulated food/unconditioned stimulus activating salivation/unconditioned response from the postsynaptic terminal, while voltage pulses applied at the back gate emulated bell/conditioned stimulus for the dog activating a conditioned response. Pavlov's dog started to salivate (unconditioned response) on noticing food (stage a, stimulus of 10 light pulses, $\lambda = 445$ nm), marked by a corresponding high-level current output above 500 nA (salivation response threshold). However, at the beginning, the bell ring (stimulus of 10 voltage pulses) alone did not lead to any salivation (current < 500 nA, data not shown). During the initial training routines (10 cycles) with simultaneous feeding and ringing the bell, the PSCs increased above the salivation response threshold. But conditioned stimulus alone still did not produce salivation, indicating inefficient response in the dog (stage b). However, on repeated training with simultaneous feeding and ringing the bell (40 cycles), the dog learned to associate the ring (conditioned stimulus) with food (unconditioned stimulus), marked by postsynaptic currents higher than the salivation response threshold (stage c, d). Conditioned response after the 40 training cycles remained so strong that subsequent conditioned stimulus alone clearly produced a high current output higher than the salivation threshold for ≈2 h, indicating an efficient association (learning) between the food/unconditioned stimulus and the bell/conditioned stimulus (stage e, f). As a result, Pavlov's dog now salivated when it heard the ringing of the bell alone. Important classical conditioning signatures of extinction and recovery[71] were also realized in our system. A series of voltage pulses (conditioned stimuli) applied to the "well-trained" dog without accompanying unconditioned stimuli, resulted in decrease of PSC (mimicking depression) below the salivation threshold after ≈2 h. This extinction process (stage g) correlated with the elimination of old information in the human brain. This conditioned reflex was again rebuilt or recovered on additional "retraining" (stage h). It was observed that the number of retraining cycles (15) required to reaccomplish the same level of association was less than the initial number of training cycles (20). This in-turn reflected a semipermanent conductance change due to excessive electron accumulation on repeated learning.

In summary, comprehensive synaptic behaviors were demonstrated for the first time in 2D MoS_2 three-terminal devices with a synergistic multigate architecture exhibiting three modes of operation, namely, electronic, ionotronic, and photoactive. The memory behavior was linked to the origin of hysteresis and was attributed to electron trapping–detrapping at the semiconducting channel, migration–relaxation of ions in the IL gate dielectric, and slow trap assisted recombination depending on the configuration. Presynaptic voltage stimuli first activated STP/STD in our artificial synapse and persistent voltage/optical stimuli consolidated the resistance state to achieve LTP/LTD. Synaptic plasticity was tuned by modulating temporal correlations between presynaptic and postsynaptic action potentials and the three modes were combined to modulate Hebbian STDP plasticity with metaplasticity and homeostatic regulation. Vital characteristics of neurotransmitter release and dynamic logic was realized using frequency, amplitude, and synchronicity dependent pulsing algorithms. Finally, classical conditioning was emulated using simultaneous paired stimulation of unconditioned optical and conditioned voltage pulses, resulting in associative learning. Furthermore, the inculcated conditioned response could be extinguished, and recovered under continuous conditioned stimulation and retraining. Compared to previously reported artificial electrical synapses, such optoelectronic synapses pave the way for intelligent optical computing systems with ultrafast propagation speed without interconnect issues, and selective activation of neurons and synapses similar to optogenetics. The metaplasticity effect potentially alleviates a lot of network level issues pertaining to statistical variations between synaptic and neuronal elements. However, some of the challenges which have to be overcome for large-scale usage of this technology include development of reliable integration with underlying CMOS electronics, ionically gating large array of transistors and managing the differences in voltage amplitudes between the difference modes of operation.

Experimental Section

A scotch-tape method was used to exfoliate MoS_2 flakes from bulk crystal and was transferred onto a degenerately doped Si substrate with 285 nm SiO_2. The thin flakes were identified by optical contrast conducted with Olympus BX51 microscope. Raman and photoluminescence characterizations were performed using Witec confocal Raman system under 532 nm laser excitation. The electrodes were patterned via photolithography, followed by thermal evaporation of Cr/Au (5/50 nm) and subsequent lift-off process. Electrical measurements were carried out using Keithley 4200-SCS semiconductor characterization system via custom defined pulsing programs with a coupled light source (Thorlabs Solis-445C) and a DC2200 driver in an external transistor–transistor logic modulation configuration.

Supporting Information

Supporting Information is available from the Wiley Online Library or from the author.

Acknowledgements

R.A.J. and F.L. contributed equally to this work. The authors would like to acknowledge the funding from MOE Tier 1 grant RG 166/16, MOE Tier 2 grants MOE2016-T2-1-100 and MOE2015-T2-2-007, and from National Research Foundation under NRF RF Award No. NRF-RF2013-08.

Note: Figure 2 was replaced on June 15, 2018, after initial publication online, as Figure 2F–H, which show asymmetric Hebbian, asymmetric anti-Hebbian, and symmetric Hebbian behavior, were mislabeled. The caption was also updated, together with the sentences on page 5 "While operation in the electronic-mode helped..." and on page 7, "Staying within this time frame, the corresponding STDP protocol..." of the main text. The final conclusions of the work are unaffected.

Conflict of Interest

The authors declare no conflict of interest.

Keywords

2D chalcogenides, associative learning, Hebbian synaptic plasticity, homeostatic regulation, neuromorphic computing

Received: January 10, 2018
Revised: February 25, 2018
Published online: May 4, 2018

[1] M. M. Waldrop, *Nature* **2012**, *482*, 456.
[2] S. Herculano-Houzel, *Front. Hum. Neurosci.* **2009**, 3.
[3] L. F. Abbott, S. B. Nelson, *Nat. Neurosci.* **2000**, *3*, 1178.
[4] W. Gerstner, W. M. Kistler, R. Naud, L. Paninski, *Neuronal Dynamics: From Single Neurons to Networks and Models of Cognition*, Cambridge University Press, Cambridge **2014**.
[5] R. Gopalakrishnan, A. Basu, *IEEE Trans. Neural Netw. Learn. Syst.* **2017**, *28*, 778.
[6] G. Indiveri, S.-C. Liu, *Proc. IEEE* **2015**, *103*, 1379.
[7] Z. Wang, S. Joshi, S. E. Savel'ev, H. Jiang, R. Midya, P. Lin, M. Hu, N. Ge, J. P. Strachan, Z. Li, *Nat. Mater.* **2017**, *16*, 101.
[8] T. Ohno, T. Hasegawa, T. Tsuruoka, K. Terabe, J. K. Gimzewski, M. Aono, *Nat. Mater.* **2011**, *10*, 591.
[9] M. Prezioso, F. Merrikh-Bayat, B. D. Hoskins, G. C. Adam, K. K. Likharev, D. B. Strukov, *Nature* **2015**, *521*, 61.
[10] G. Indiveri, B. Linares-Barranco, T. J. Hamilton, A. Van Schaik, R. Etienne-Cummings, T. Delbruck, S.-C. Liu, P. Dudek, P. Häfliger, S. Renaud, *Front. Neurosci.* **2011**, *5*, 73.
[11] Y. van de Burgt, E. Lubberman, E. J. Fuller, S. T. Keene, G. C. Faria, S. Agarwal, M. J. Marinella, A. A. Talin, A. Salleo, *Nat. Mater.* **2017**, *16*, 414.
[12] Y. Zang, H. Shen, D. Huang, C. Di, D. Zhu, *Adv. Mater.* **2017**, *29*, 1606088.
[13] P. Gkoupidenis, D. A. Koutsouras, G. G. Malliaras, *Nat. Commun.* **2017**, *8*, 15448.
[14] J. Shi, S. D. Ha, Y. Zhou, F. Schoofs, S. Ramanathan, *Nat. Commun.* **2013**, *4*, 3676.
[15] L. Q. Zhu, C. J. Wan, L. Q. Guo, Y. Shi, Q. Wan, *Nat. Commun.* **2014**, *5*, 4158.
[16] R. A. John, J. Ko, M. R. Kulkarni, N. Tiwari, N. A. Chien, N. Geok, W. L. Leong, N. Mathews, *Small* **2017**, *13*, 1701193.
[17] X. Hong, J. Kim, S.-F. Shi, Y. Zhang, C. Jin, Y. Sun, S. Tongay, J. Wu, Y. Zhang, F. Wang, *Nat. Nanotechnol.* **2014**, *9*, 682.
[18] B. Radisavljevic, A. Radenovic, J. Brivio, I. V. Giacometti, A. Kis, *Nat. Nanotechnol.* **2011**, *6*, 147.
[19] K. Kang, S. Xie, L. Huang, Y. Han, P. Y. Huang, K. F. Mak, C.-J. Kim, D. Muller, J. Park, *Nature* **2015**, *520*, 656.
[20] S. Mouri, Y. Miyauchi, K. Matsuda, *Nano Lett.* **2013**, *13*, 5944.
[21] H. J. Conley, B. Wang, J. I. Ziegler, R. F. Haglund Jr, S. T. Pantelides, K. I. Bolotin, *Nano Lett.* **2013**, *13*, 3626.
[22] N. Vitureira, Y. Goda, *J. Cell Biol.* **2013**, *203*, 175.
[23] A. M. Shen, C.-L. Chen, K. Kim, B. Cho, A. Tudor, Y. Chen, *ACS Nano* **2013**, *7*, 6117.
[24] A. J. Arnold, A. Razavieh, J. R. Nasr, D. S. Schulman, C. M. Eichfeld, S. Das, *ACS Nano* **2017**, *11*, 3110.
[25] J. Jiang, J. Guo, X. Wan, Y. Yang, H. Xie, D. Niu, J. Yang, J. He, Y. Gao, Q. Wan, *Small* **2017**, *13*, 1700933.
[26] S. Nakanishi, *Science* **1992**, *258*, 597.
[27] J. Del Castillo, B. Katz, *J. Physiol.* **1954**, *124*, 560.
[28] T. Branco, K. Staras, *Nat. Rev. Neurosci.* **2009**, *10*, 373.
[29] R. S. Zucker, *Annu. Rev. Neurosci.* **1989**, *12*, 13.
[30] J. C. López, *Nat. Rev. Neurosci.* **2001**, *2*, 307.
[31] G. Perea, A. Araque, *Science* **2007**, *317*, 1083.
[32] J. T. Coyle, P. Puttfarcken, *Science* **1993**, *262*, 689.
[33] M. A. Castro-Alamancos, B. W. Connors, *Proc. Natl. Acad. Sci. USA* **1996**, *93*, 1335.
[34] G. Buzsáki, A. Draguhn, *Science* **2004**, *304*, 1926.
[35] L. F. Abbott, W. G. Regehr, *Nature* **2004**, *431*, 796.
[36] J. M. J. Murre, J. Dros, *PLoS One* **2015**, *10*, e0120644.
[37] A. N. Burkitt, *Biol. Cybern.* **2006**, *95*, 97.
[38] A. N. Burkitt, *Biol. Cybern.* **2006**, *95*, 1.
[39] W. Xu, H. Cho, Y. H. Kim, Y. T. Kim, C. Wolf, C. G. Park, T. W. Lee, *Adv. Mater.* **2016**, *28*, 5916.
[40] F. S. Chance, L. F. Abbott, A. D. Reyes, *Neuroendocrinology* **2002**, *35*, 773.
[41] E. Salinas, P. Thier, *Neuroendocrinology* **2000**, *27*, 15.
[42] W. Xu, S.-Y. Min, H. Hwang, T.-W. Lee, *Sci. Adv.* **2016**, *2*, e1501326.
[43] G.-H. Lee, Y.-J. Yu, X. Cui, N. Petrone, C.-H. Lee, M. S. Choi, D.-Y. Lee, C. Lee, W. J. Yoo, K. Watanabe, *ACS Nano* **2013**, *7*, 7931.
[44] I. Gupta, A. Serb, A. Khiat, R. Zeitler, S. Vassanelli, T. Prodromakis, *Nat. Commun.* **2016**, *7*, 12805.
[45] G. Narasimman, S. Roy, X. Fong, K. Roy, C.-H. Chang, A. Basu, in *2016 IEEE Int. Symp. on Circuits Syst. (ISCAS)*, IEEE, Montreal **2016**, pp. 914–917.
[46] G. L. Collingridge, T. V. P. Bliss, *Trends Neurosci.* **1987**, *10*, 288.
[47] H. Tian, Q. Guo, Y. Xie, H. Zhao, C. Li, J. J. Cha, F. Xia, H. Wang, *Adv. Mater.* **2016**, *28*, 4991.
[48] I. Amit, T. J. Octon, N. J. Townsend, F. Reale, C. D. Wright, C. Mattevi, M. F. Craciun, S. Russo, *Adv. Mater.* **2017**, *29*, 05598.
[49] O. Lopez-Sanchez, D. Lembke, M. Kayci, A. Radenovic, A. Kis, *Nat. Nanotechnol.* **2013**, *8*, 497.
[50] D. Kufer, G. Konstantatos, *Nano Lett.* **2015**, *15*, 7307.
[51] K. Roy, M. Padmanabhan, S. Goswami, T. P. Sai, G. Ramalingam, S. Raghavan, A. Ghosh, *Nat. Nanotechnol.* **2013**, *8*, 826.
[52] Y.-C. Wu, C.-H. Liu, S.-Y. Chen, F.-Y. Shih, P.-H. Ho, C.-W. Chen, C.-T. Liang, W.-H. Wang, *Sci. Rep.* **2015**, *5*, 11472.
[53] T. V Bliss, G. L. Collingridge, *Nature* **1993**, *361*, 31.
[54] W. C. Abraham, M. F. Bear, *Trends Neurosci.* **1996**, *19*, 126.
[55] S. Song, K. D. Miller, L. F. Abbott, *Nat. Neurosci.* **2000**, *3*, 919.
[56] S. Brink, S. Nease, P. Hasler, S. Ramakrishnan, R. Wunderlich, A. Basu, B. Degnan, *IEEE Trans. Biomed. Circuits Syst.* **2013**, *7*, 71.
[57] E. Edelmann, E. Cepeda-Prado, V. Leßmann, *Front. Synaptic Neurosci.* **2017**, *9*, 7.
[58] G. G. Turrigiano, S. B. Nelson, *Nat. Rev. Neurosci.* **2004**, *5*, 97.
[59] K. Pozo, Y. Goda, *Neuroendocrinology* **2010**, *66*, 337.
[60] F. Zenke, E. J. Agnes, W. Gerstner, *Nat. Commun.* **2015**, *6*, 6922.
[61] X. Zhu, C. Du, Y. Jeong, W. D. Lu, *Nanoscale* **2017**, *9*, 45.
[62] Z. Tan, R. Yang, K. Terabe, X. Yin, X. Zhang, X. Guo, *Adv. Mater.* **2016**, *28*, 377.
[63] N. Frémaux, W. Gerstner, *Front. Neural Circuits* **2016**, *9*, 85.
[64] V. Pawlak, J. R. Wickens, A. Kirkwood, J. N. D. Kerr, *Front. Synaptic Neurosci.* **2010**, *2*, 146.
[65] A. J. Watt, N. S. Desai, *Front. Synaptic Neurosci.* **2010**, *2*, 5.
[66] C. Clopath, L. Büsing, E. Vasilaki, W. Gerstner, *Nat. Neurosci.* **2010**, *13*, 344.
[67] T. Serrano-Gotarredona, T. Masquelier, T. Prodromakis, G. Indiveri, B. Linares-Barranco, *Front. Neurosci.* **2013**, *7*, 2.
[68] S. Ramakrishnan, P. E. Hasler, C. Gordon, *IEEE Trans. Biomed. Circuits Syst.* **2011**, *5*, 244.
[69] I. P. Pavlov, G. V. Anrep, *Conditioned Reflexes*, Courier Corporation, **2003**.
[70] Z.-H. Tan, X.-B. Yin, R. Yang, S.-B. Mi, C.-L. Jia, X. Guo, *Sci. Rep.* **2017**, *7*, 713.
[71] C. Wu, T. W. Kim, T. Guo, F. Li, D. U. Lee, J. J. Yang, *Adv. Mater.* **2017**, *29*, 1602890.

